IEEE Access
Multidisciplinary | Rapid Review | Open Access Journal

Received October 23, 2019, accepted October 30, 2019, date of publication November 5, 2019, date of current version November 15, 2019.

Digital Object Identifier 10.1109/ACCESS.2019.2951583

Contrast Enhancement Using Sensitivity Model-Based Sigmoid Function

SEUNG PARK, YONG-GOO SHIN, AND SUNG-JEA KO, (Fellow, IEEE)
School of Electrical Engineering, Korea University, Seoul 02841, South Korea

Corresponding author: Sung-Jea Ko (sjko@korea.ac.kr)

This work was supported in part by the Institute for Information and Communications Technology Promotion (IITP) through the Ministry of Science and ICT (MSIT) of Korea Government under Grant 2017-0-00250, and in part by the Intelligent Defense Boundary Surveillance Technology Using Collaborative Reinforced Learning of Embedded Edge Camera and Image Analysis.

ABSTRACT For indirect contrast enhancement, researchers have proposed various transformation functions based on histogram equalization and gamma correction. However, these transformation functions tend to result in over-enhancement artifacts such as noise amplification, mean brightness change, and detail loss. To overcome the limitations of conventional transformation functions, this paper introduces a novel sigmoid function based on the contrast sensitivity of human brightness perception. In the proposed method, the contrast sensitivity of the human retina is modeled as an exponential function of the log-intensity, and a transformation function is derived using the sensitivity model as the exponent of Steven's power law. We also present a parameter optimization method that maintains the mean brightness of the input image and stretches the image histogram while minimizing information loss. Experimental results demonstrate that the proposed method has low computational complexity and outperforms the state-of-the-art methods in terms of contrast enhancement performance, mean brightness preservation, and detail preservation.

INDEX TERMS Contrast enhancement, sensitivity model-based sigmoid function, Steven's power law.

I. INTRODUCTION

Digital images often have low contrast owing to inadequate image capture devices or undesirable lighting conditions. Since low contrast images may have a washed-out appearance or do not reveal all the scene details [1], researchers have proposed various enhancement methods to improve the visual quality of these images [2], [3].

Contrast enhancement techniques are broadly classified into two groups: direct and indirect methods [4]. In direct methods [5]–[8], image contrast is measured based on the human visual system (HVS), such as the Weber–Fechner law or Retinex theory [9], and is improved by applying various nonlinear functions [5], [6] or solving optimization problems [7], [8]. Direct methods have some advantages of image detail enhancement as well as dynamic range compression, however, they require high computational complexity and introduce "halo" artifacts particularly around strong edges [10], [11]. Although recent direct methods have been proposed [38], [48], [49], [60]–[63] to alleviate these problems, it is still challenging to provide both high image contrast and real-time processing without causing noticeable distortion. For these reasons, indirect methods utilizing a global transformation function are more widely employed in practical applications than direct methods.

One of the most representative indirect methods, histogram equalization (HE) produces visual artifacts such as noise amplification, contouring, or significant brightness change when there are high peak values in the image histogram [1]. To alleviate these problems, many HE-based methods modify the image histogram to attenuate the high peak values and then derive the transformation function from the modified histogram. In [1], the image histogram was combined with a uniform distribution by solving a bi-criteria optimization problem. Kim and Chung [12] utilized a normalized power-law function to smoothen high peak values in the image histogram. Since HE shifts the mean brightness of the enhanced image to the middle gray level, researchers have separated the image histogram into multiple sub-histograms and performed HE on each sub-histogram individually [12]–[16]. For detail preservation, recent indirect methods utilize a two-dimensional (2D) histogram [19]–[21], [51], [52] or fuzzy contextual information [45], [53] to build the image histogram which gives more weight to the pixels in texture

The associate editor coordinating the review of this manuscript and approving it for publication was Huanqiang Zeng.

regions. Compared with other indirect methods, these methods achieve better enhancement performance and less information loss.

More recently, deep learning-based methods, especially Convolutional Neural Networks (CNNs), have been extensively researched for image enhancement. In our best knowledge, however, most deep learning-based methods have been developed for medical images [54], [55], low-light images [56], [57], or hazed images [58], [59] rather than natural image enhancement.

In this paper, we first introduce a novel sigmoid function based on the contrast sensitivity of human brightness perception. Motivated by the observation that the contrast sensitivity of the human retina decreases exponentially as the log-luminance increases, we model the contrast sensitivity as an exponential function of the log-intensity level. Using the contrast sensitivity model, the sigmoid function is derived by modifying the exponent of Steven's power law. We also present a parameter optimization method that maintains the mean brightness of the input image and stretches the image histogram while minimizing information loss. This process requires low computational complexity and exhibits high enhancement performance while preserving the mean brightness and details of the input image. Experimental results indicate that the proposed method outperforms the state-of-the-art methods with regard to mean brightness preservation, detail preservation, and contrast enhancement performance. Objective image quality evaluation also confirms that the proposed method provides excellent visual quality.

The remainder of this paper is organized as follows: Section II describes human brightness perception and its applications for contrast enhancement. Section III explains the proposed method in detail. Section IV discusses the experimental results to demonstrate the performance and characteristics of the proposed method, and lastly, Section V concludes the paper.

II. BACKGROUND

A. HUMAN BRIGHTNESS PERCEPTION

The photoreceptors in the human retina, which are called rods and cones, operate as the sensors for the HVS. Rods are very sensitive to light and provide achromatic vision named scotopic vision at low luminance levels (10^{-6} to 10cd/m^2). At luminance levels higher than 10^{-2}cd/m^2, rods begin to saturate and cones provide chromatic vision named photopic vision. At luminance levels between 10^{-2} and $10\ \text{cd/m}^2$, both rods and cones are active and the human retina operates in a transition mode called mesopic vision. Since neurons can only transfer a signal with a dynamic range of approximately $1:10^3$, the human retina compresses the dynamic range of the real-scene luminance by adapting to a certain luminance level called the adaptation level and then perceiving images in a rather small dynamic range around the adaptation level. To describe the retinal response of human brightness perception, various response models based on neuroscience experiments have been proposed.

One of the representative response models—the Naka-Rushton equation—describes the relationship between the retinal response R and the luminance level L, which is given by

$$R(L) = \frac{L^n}{L^n + \sigma^n}, \tag{1}$$

where n is a parameter determining the steepness of the retinal response function and σ is the adaptation level. Eq. (1) indicates that the HVS transforms the luminance level into the retinal response by employing a sigmoid curve centered on the adaptation level. Recent tone mapping techniques generally employ the sigmoid curve as a camera response function which converts real-world radiance into pixel intensity [33]–[37]. Using the human brightness perception-based sigmoid curve, these methods achieve high contrast performance while avoiding visual artifacts.

B. HUMAN PERCEPTION-BASED INDIRECT METHODS

Many indirect methods derive their transformation functions using the just noticeable difference (JND), which is the minimum luminance difference that the human retina can perceive. According to the Weber-Fechner law, the JND, dL/dS, is proportional to the background luminance L, as follows:

$$\frac{dL}{dS} = kL, \tag{2}$$

where k is a perceptual constant called the Weber fraction. From Eq. (2), the perceived brightness S can be expressed as

$$S = \frac{1}{k}\log_e L + S_0, \tag{3}$$

where S_0 is the integral constant. Motivated by Eq. (3), various indirect methods use a logarithmic function [38] or a GC [23]–[26] as the transformation function. However, these functions do not match the retinal response function at low luminance levels because the Weber-Fechner law only holds for luminance levels greater than 10^2cd/m^2 [39]. For this reason, they often introduce over-enhancement in dark regions. To alleviate this problem by assigning a larger dynamic range to highly-populated luminance levels, Huang *et al.* [23] proposed an adaptive gamma correction (AGC) method that determines the gamma parameter by using the image histogram. In this method, the transformation function $R(L)$ is given as

$$R(L) = \left(\frac{L}{L_{\max}}\right)^{1-\text{CDF}(L)}, \tag{4}$$

where $L_{\max}$ is the maximum pixel intensity and $\text{CDF}(L)$ is the cumulative distribution function of the input histogram. The AGC method exhibits better performance than other indirect methods, particularly for dimmed images. However, this method increases the mean brightness of the image and yields over-enhancement in dark regions and detail loss in bright regions. To resolve these limitations, recently proposed methods construct a sigmoid curve by modifying the GC curve [25], [26]; however, these methods have difficulty in

determining the optimal parameter to achieve satisfactory enhancement performance and mean brightness preservation at the same time.

Meanwhile, Hassan and Akamatsu [46] proposed a sigmoid function-based transformation function $R(L)$ which is defined as

$$R(L) = L \times \left(1 + C \times \frac{1}{1 + \exp(-L)}\right), \tag{5}$$

where C is a scale parameter for determining the degree of enhancement. Motivated by this approach, Lal and Chandra [47] extended the work in [46] by modifying Eq. (5) as follows:

$$R(L) = L + K_1 \times \frac{L}{1 - \exp(K_1 \times (K_2 + L))}, \tag{6}$$

where K_1 and K_2 are tuning parameters. Although these methods demonstrated the feasibility of the sigmoid curve in contrast enhancement, they still suffer from a weak performance as well as significant image distortion.

III. PROPOSED METHOD

A. SENSITIVITY MODEL-BASED SIGMOID FUNCTION

Stevens' power law [32] is a well-known stimulus-response model that covers a wider range of sensations compared with the Weber-Fechner law. In Steven's power law, the perceived brightness $R(L)$ is given by

$$R(L) = L^k, \tag{7}$$

where the exponent k depends on the type of stimulation. In the differential form, Eq. (7) can be rewritten as

$$\frac{1}{R}dR = k\frac{1}{L}dL. \tag{8}$$

As shown in Eq. (8), k works as a sensitivity parameter determining how fast the sensation grows as the stimulus intensity increases. For various types of sensations, k is assumed as a constant, resulting in the conventional GC curve. However, because the contrast sensitivity of the human retina is adaptively determined by the background luminance, we model k according to human brightness perception. As illustrated in Fig. 1, Wyszecki and Stiles [31] showed experimentally that the contrast sensitivity of human brightness perception, *i.e.*, the Weber fraction, decreases exponentially as the log-luminance increases. The fitting curve in Fig. 1 indicates that the Weber fraction can be approximated as an exponential function of the log-luminance. Based on these observations, we model k as the following exponential function:

$$k(L) = \alpha\beta^{-\log_e(L)}, \tag{9}$$

where α and β are parameters determining the maximum value and steepness of $k(L)$, respectively. By substituting Eq. (9) into Eq. (7) and multiplying by 255, the transformation function $R(L)$ is given as

$$R(L) = 255 \times \tilde{L}^{\alpha\beta^{-\log_e(\tilde{L})}}. \tag{10}$$

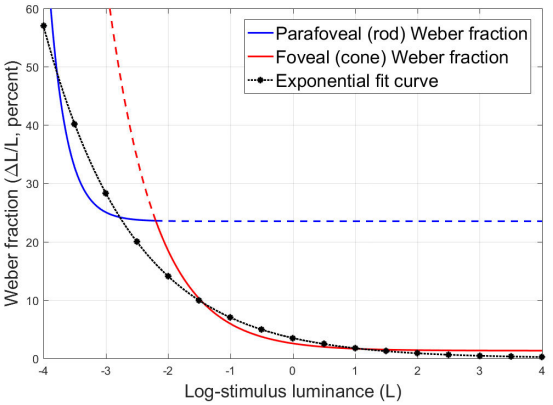

FIGURE 1. Weber fraction for different luminance levels. The left (blue line) and right (red line) parts correspond to scotopic and mesopic vision, respectively. The fitting curve (dark line) shows that the Weber fraction can be approximated using an exponential function of the log-luminance.

In Eq. (10), L is the original pixel intensity in the range of [0, 255] and $\tilde{L}$ is the pixel intensity normalized to [0, 1] which is obtained by

$$\tilde{L} = \frac{L - L_{\min}}{L_{\max} - L_{\min}}, \tag{11}$$

where $L_{\min}$ and $L_{\max}$ are the minimum and maximum intensity levels of the input image, respectively. Note that we set $R\left(\tilde{L}\right)$ for $\tilde{L} = 0$ as zero to avoid the singularity problem. The transformation function in Eq. (10) covers the full dynamic range $[R(L_{\min}) = 0, R(L_{\max}) = 255]$ of a digital image.

B. AUTOMATIC PARAMETER ESTIMATION

The proposed transformation function in Eq. (10) has two parameters, *i.e.* α and β. In this subsection, we analyze the influence of these parameters on the resultant images and introduce a novel automatic parameter estimation method. First, we compared the output images obtained by varying α from 0.3 to 1.1 with increments of 0.2 while keeping β as 2.0. As shown in Fig. 2, when α increases, the output image becomes darker. This observation indicates that the mean brightness of the output image can be adjusted by controlling α; α needs some constraints to avoid image distortions and flickering artifacts caused by mean-brightness change [29], [30]. To this end, we constrained the transformation function to maintain the mean intensity level L_{mean} of the original image as follows:

$$R(L_{\text{mean}}) = 255 \times \tilde{L}_{\text{mean}}^{\alpha\beta^{-\log_e(\tilde{L}_{\text{mean}})}} = L_{\text{mean}}, \tag{12}$$

where $\tilde{L}_{\text{mean}}$ is the mean intensity level of the normalized input image. By solving Eq. (12) with respect to α, optimal α for mean-brightness preservation can be obtained as follows:

$$\alpha = \frac{\log_e(L_{\text{mean}}/255)}{\log_e(\tilde{L}_{\text{mean}})} \times \beta^{\log_e(\tilde{L}_{\text{mean}})}. \tag{13}$$

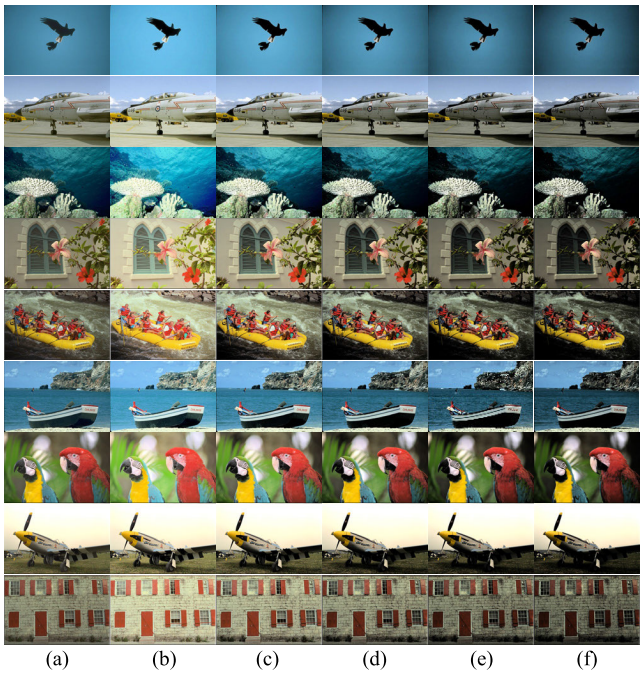

FIGURE 2. Impacts of the parameter α on the output images: (a) input images, (b)-(f) output images at $\alpha = 0.3, 0.5, 0.7, 0.9$, and 1.1, respectively. For all images, β was fixed as 2.0.

As illustrated in Fig. 3(g), the transformation function with α obtained via Eq. (13) maintains the mean intensity level of the input image regardless of β value.

We also conducted extensive experiments to analyze the effects of β on the output images by varying β from 1.0 to 3.0 with increments of 0.5. For these experiments, we set α using Eq. (13). As indicated in Fig. 3, β controls the enhancement degree by determining the steepness of the transformation function. When β is too small, the enhancement performance of the proposed method is unsatisfactory. On the other hand, if β is too large, the transformation function has a steep slope resulting in significant detail loss in dark and bright regions. Therefore, to estimate optimal β that improves the image contrast while preserving the image detail, we define the following cost function for parameter optimization:

$$E(\beta, \lambda) = E_d(\beta) - \lambda E_e(\beta), \tag{14}$$

where $E_d(\beta)$ is the data fidelity term, $E_e(\beta)$ is the enhancement term, and λ is the regularization parameter controlling the trade-off between the data fidelity term and enhancement term.

To prevent information loss due to the truncation of the output pixel values, E_d is defined as the discrete entropy (DE) loss:

$$E_d(\beta) = -\sum_{k=1}^{N} p(h_{i,k}) \log_2 p(h_{i,k}) + \sum_{k=1}^{N} p(h_{o,k}) \log_2 p(h_{o,k}), \tag{15}$$

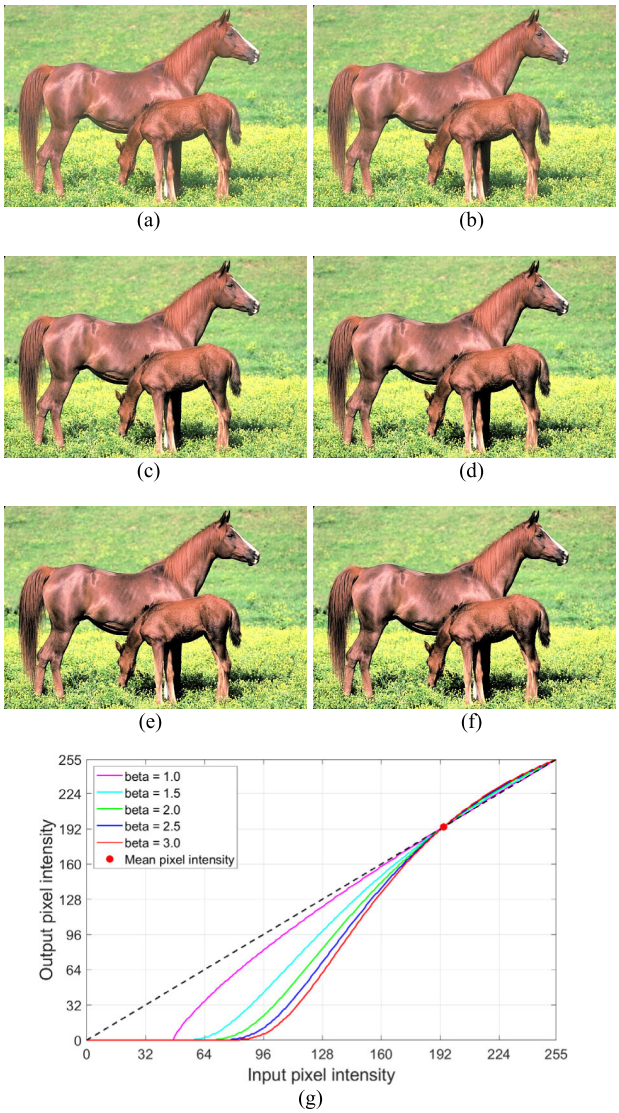

FIGURE 3. Effects of the parameter β on the output images: (a) input image, (b)-(f) output images at $\beta = 1.0$ (conventional gamma curve), 1.5, 2.0, 2.5, and 3.0 respectively, and (g) corresponding transformation functions with the mean brightness of the input image (red circle). For all images, α was estimated by using Eq. (13) for mean brightness preservation.

where $p(\cdot)$ is the probability mass function, h_i is the k-th bin of the original histogram, and h_o is the output histogram obtained by using Eq. (10) with given β.

For the enhancement term, we employ PixDist method [40] which measures the gray-level difference of all pixels in the image:

$$E_e(\beta) = \frac{1}{N(N-1)} \sum_{i=1}^{N} \sum_{j=i}^{N} h_o(i)\, h_o(j)(j-i). \tag{16}$$

This term results in a high score when the image histogram is uniformly distributed without being concentrated in particular gray-levels. To find optimal β minimizing the cost function $E(\beta)$ in Eq. (14), we employ the golden section search algorithm [50] which evaluates $E(\beta)$ at triples of

points whose values form the golden ratio and successively narrows the search interval. In this algorithm, we use the initial interval as [1.2, 2.4] and the iteration process continues until the bracketing interval $[\beta_l, \beta_u]$ is tolerably small $\left(\beta_u - \beta_l < 10^{-4}\right)$ or a maximal number of iterations is reached ($K_{\max} = 500$).

IV. EXPERIMENTAL RESULTS

550 test images were taken from three datasets in [41]–[43] for a comparison of the proposed method (sensitivity model-based sigmoid curve, SMSC) with weighted adaptive histogram equalization (WAHE) [1], contextual and variational contrast (CVC) [20], layered difference representation (LDR) [11], adaptive gamma correction (AGC) [23], fuzzy-contextual contrast enhancement (FCCE) [45], two sigmoid function-based methods [46], [47], and some recent direct methods [38], [48], [49]. The conventional methods are implemented by employing the default parameters provided by the authors. The average processing time is tested on each dataset using a desktop machine with Intel i5-3550 3.30 GHz CPU and 8GB RAM.

To determine the optimal value for the parameter λ, we first tested the proposed method on the Berkeley image dataset [43] by changing λ from 0 to 0.05 with 0.001 steps as demonstrated in Fig. 4. For large λ, the proposed method provided considerable improvement in image contrast as shown in PixDist scores, but resulted in significant detail loss as indicated in DE scores. To achieve high enhancement performance while preventing detail loss, λ was empirically set as 0.015 for objective and subjective assessments. To prevent color distortion, the image was first converted to the *HSV* color space, and only the luminance channel V was processed, while the H and S channels remained unchanged.

A. OBJECTIVE ASSESSMENT

For an objective assessment, we employed the measure of contrast enhancement (EME) [3], absolute mean brightness error (AMBE) [30], gradient magnitude similarity deviation (GMSD) [44], and discrete entropy (DE) measures. Table 1 shows the average test image performance with the average processing time for each of the datasets. The best and second-best results in each category are in bold and underlined, respectively Owing to space limitations in the table, we omitted the standard deviation of the data.

First, EME measures the average contrast of an image based on Weber contrast. For EME, the enhanced image X was divided into N sub-blocks $X_{i,j}$ of size $w \times h$, and the ratio of maximum to minimum gray-level of each sub-block was calculated. Then, the average ratio is calculated as the final score. The EME is computed as:

$$\mathrm{EME}(X) = \frac{1}{W \times H} \sum_{i=1}^{W} \sum_{j=1}^{H} 20 \ln \frac{\max(X_{i,j})}{\min\left(X_{i,j}\right) + \delta}, \quad (17)$$

where $\max(X_{i,j})$ and $\min(X_{i,j})$ are the maximum and minimum pixel intensities in sub-block $X_{i,j}$, respectively.

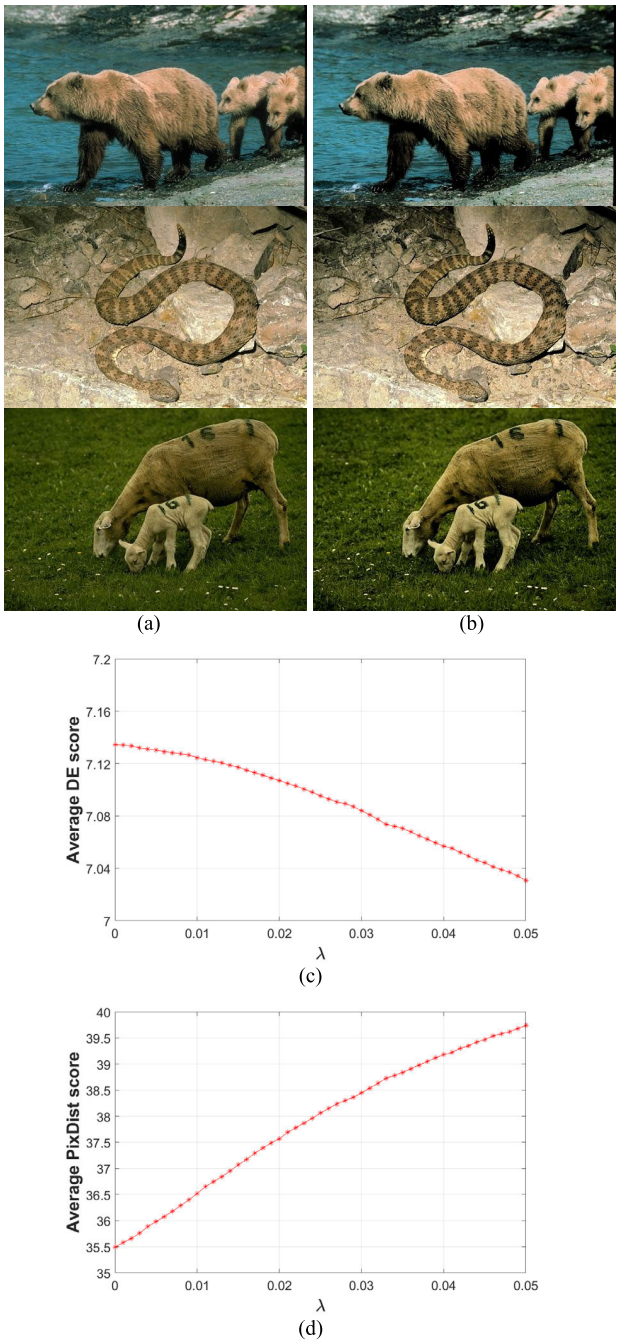

FIGURE 4. Effects of the parameter λ of the proposed method on the enhanced images obtained by using Berkeley image dataset [43]: (a)-(b) output images at λ = 0 and 0.05, respectively, (c) average discrete entropy (DE) scores, and (d) average PixDist [40] scores.

In Eq. (17), δ was set as 0.0001 to avoid division by zero and $w \times h$ was set as 8×8.

Second, AMBE measures the absolute difference of mean pixel intensities between the input and enhanced images as follows:

$$\mathrm{AMBE}(X, Y) = \frac{1}{W \times H} \sum_{i=1}^{W} \sum_{j=1}^{H} |Y(i,j) - X(i,j)|, \quad (18)$$

TABLE 1. Objective assessment of enhancement methods using the four measures: Measure of Contrast Enhancement (EME) [3], Absolute Mean Brightness Error (AMBE) [30], Gradient Magnitude Similarity Deviation (GMSD) [44], and discrete entropy as well as average processing times. The best and second-best results in each category are in bold and underlined, respectively.

I. Kodak Lossless True Color Image Suite [41]						
Categories	Algorithms	EME	AMBE	GMSD	DE	Processing time (ms)
Direct methods	NPEA [38]	11.50	27.29	0.0344	7.1921	9631.2
	LSCN [48]	**77.56**	14.96	0.0988	6.4947	6061.8
	RSIE [49]	24.10	**5.67**	**0.0201**	**7.4962**	302.0
Indirect methods	WAHE [1]	15.83	5.97	0.0339	7.1302	5.6
	CVC [20]	22.99	8.13	0.0349	7.1174	103.4
	LDR [11]	24.00	8.45	0.0257	7.1500	18.3
	AGC [23]	15.66	41.05	0.0690	6.8529	1.8
	FCCE [45]	21.02	9.17	0.0635	**7.5293**	121.0
	CESF [46]	13.84	50.76	0.1018	5.8133	0.3
	EACE [47]	24.84	10.18	0.1277	7.0448	35.4
	SMSF (proposed)	**26.17**	**4.66**	**0.0255**	7.1673	5.4
II. USC-SIPI Database [42]						
Categories	Algorithms	EME	AMBE	GMSD	DE	Processing time (ms)
Direct methods	NPEA [38]	12.92	21.89	0.0408	7.1388	4756.4
	LSCN [48]	**75.80**	16.71	0.0888	6.3999	2385.2
	RSIE [49]	25.97	**11.18**	**0.0344**	**7.5124**	171.0
Indirect methods	WAHE [1]	14.06	6.45	0.0349	6.9922	2.4
	CVC [20]	19.05	8.08	0.0351	6.9889	49.9
	LDR [11]	19.60	11.98	**0.0250**	7.0201	10.7
	AGC [23]	11.77	37.13	0.0556	6.7313	1.1
	FCCE [45]	20.04	9.49	0.0622	**7.4246**	43.5
	CESF [46]	9.91	51.48	0.1279	5.2123	0.2
	EACE [47]	22.68	10.88	0.1259	7.0107	34.1
	SMSF (proposed)	**29.30**	**5.28**	0.0322	7.0281	5.2
III. Berkeley Image Dataset [43]						
Categories	Algorithms	EME	AMBE	GMSD	DE	Processing time (ms)
Direct methods	NPEA [38]	12.67	26.96	0.0450	7.1921	3729.7
	LSCN [48]	**86.46**	18.35	0.0965	6.4947	1511.1
	RSIE [49]	30.04	**8.29**	**0.0279**	**7.4962**	151.0
Indirect methods	WAHE [1]	17.35	7.61	**0.0285**	7.1302	1.3
	CVC [20]	24.58	9.20	0.0418	7.1174	39.9
	LDR [11]	26.21	12.70	0.0342	7.1500	7.8
	AGC [23]	14.54	37.46	0.0740	6.8529	0.5
	FCCE [45]	23.92	12.64	0.0536	**7.5293**	26.0
	CESF [46]	12.38	46.81	0.1281	5.8133	0.2
	EACE [47]	28.25	12.87	0.1293	7.1448	21.2
	SMSF (proposed)	**32.61**	**5.43**	0.0331	7.1552	3.6

where Y is the input image. A lower AMBE score indicates that the corresponding enhancement method effectively preserved the mean-brightness of the input image.

Third, GMSD computes the pixel-wise gradient- magnitude similarity between the input and enhanced images and then measures the standard deviation of the overall gradient magnitude similarity as the final score. A lower GMSD score indicates less image distortion between the input and enhanced images.

Lastly, DE measures the amount of information in an image. A high DE score indicates that the image contains more information. Owing to the information processing inequality, the output image produced by using a global transformation function cannot have a higher DE than the input image [11].

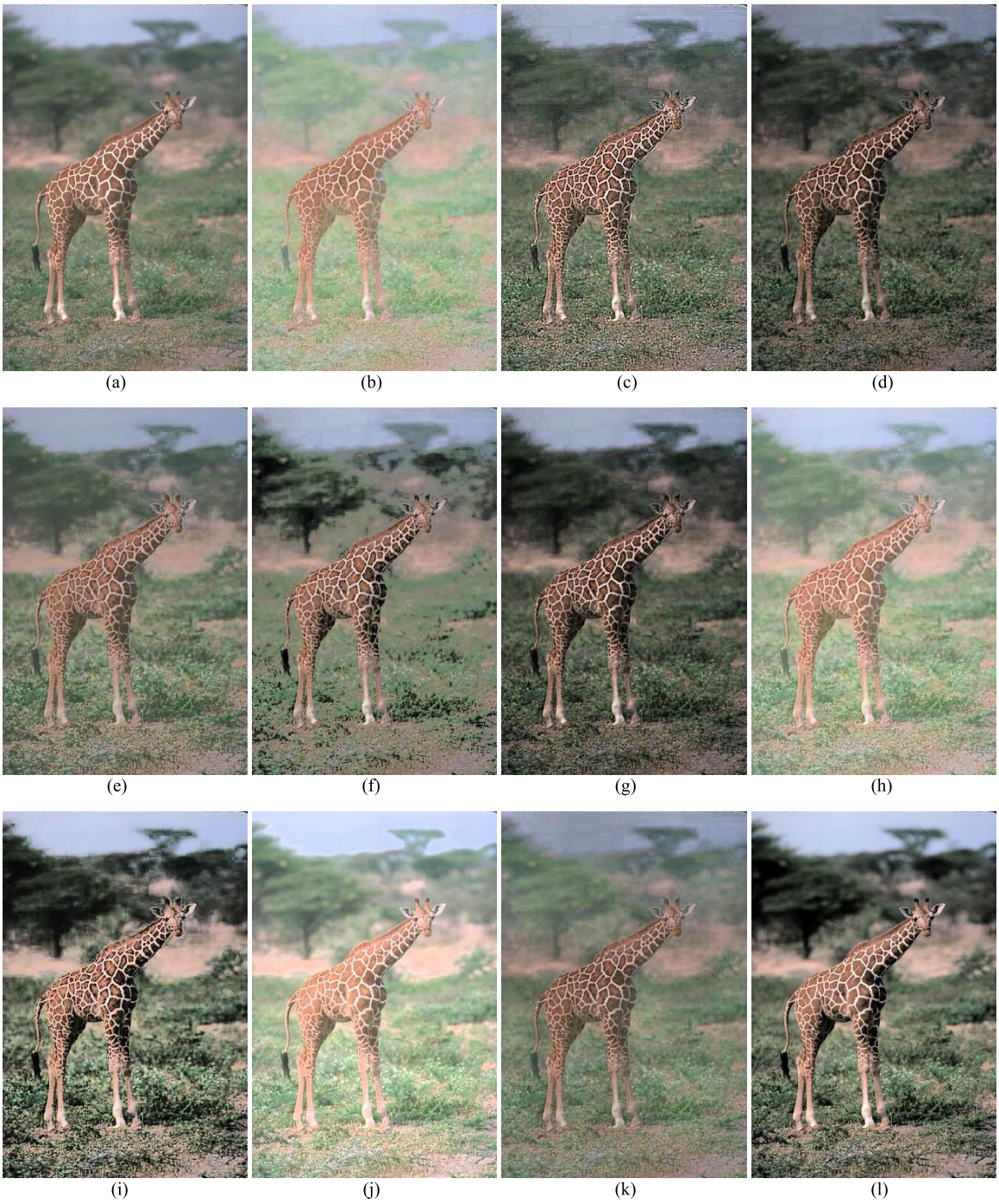

FIGURE 5. Enhanced images of the "Giraffe" image from the Berkeley image dataset [43]: (a) input image, (b) NPEA [38], (c) LSCN [48], (d) RSIE [49], (e) WAHE [1], (f) CVC [20], (g) LDR [11], (h) AGC [23], (i) FCCE [45], (j) CESF [46], (k) EACE [47], and (l) proposed method.

According to the EME results, LSCN and the proposed method exhibited the best performance in each category. However, LSCN resulted in significant image distortion as shown in GMSD scores and required much higher computational complexity than the proposed method. On the other hand, the proposed method prevented both mean-brightness change and image distortion as indicated in AMBE and GMSD scores. In addition, RSIE achieved comparable performance to the proposed method, but this method had about 50 times higher computational complexity than the proposed method.

Among the conventional indirect methods, LDR, FCCE, and EACE produced high contrast images with regard to EME scores. However, LDR showed a weak performance

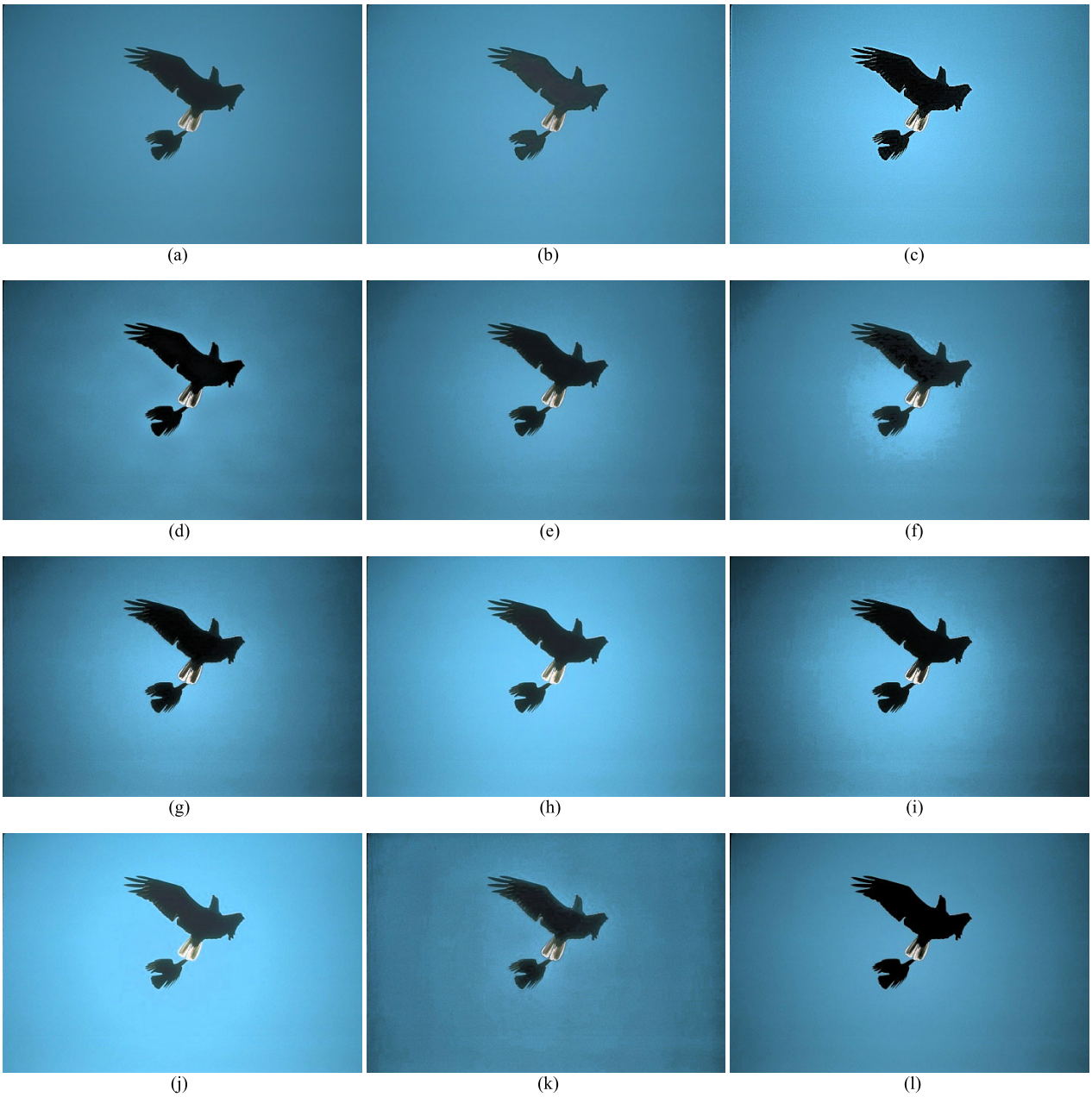

FIGURE 6. Enhanced images of the "Eagles" image from the USC-SIPI database [42]: (a) input image, (b) NPEA [38], (c) LSCN [48], (d) RSIE [49], (e) WAHE [1], (f) CVC [20], (g) LDR [11], (h) AGC [23], (i) FCCE [45], (j) CESF [46], (k) EACE [47], and (l) proposed method.

in mean-brightness preservation, especially for USC-SIPI database and Berkeley image dataset, as indicated in AMBE scores. For EACE and FCCE, the output images suffered from severe image distortion as shown in GMSD scores. In contrast, as indicated in EME scores, the proposed method achieved 16.7% better enhancement performance compared with the EACE algorithm which provided the second-best enhancement performance. In addition, the proposed method achieved 54.5% less mean-brightness change and 76.2% less image distortion than EACE as indicated in AMBE and GMSD scores, respectively. As indicated in DE scores, the proposed method demonstrated the second-best detail preservation among indirect methods. Although FCCE provided the highest DE scores, FCCE contains the local processing where the output pixel intensity is adaptively obtained by combining the input pixel intensity and the transformation function result. On the other hand, the proposed method yielded excellent DE scores without any local processing.

It is noteworthy that the proposed method achieved higher enhancement performance, lower mean-brightness change, and less image distortion with lower computational complexity at the same time compared with CVC, LDR, and FCCE which construct their transformation functions by using the

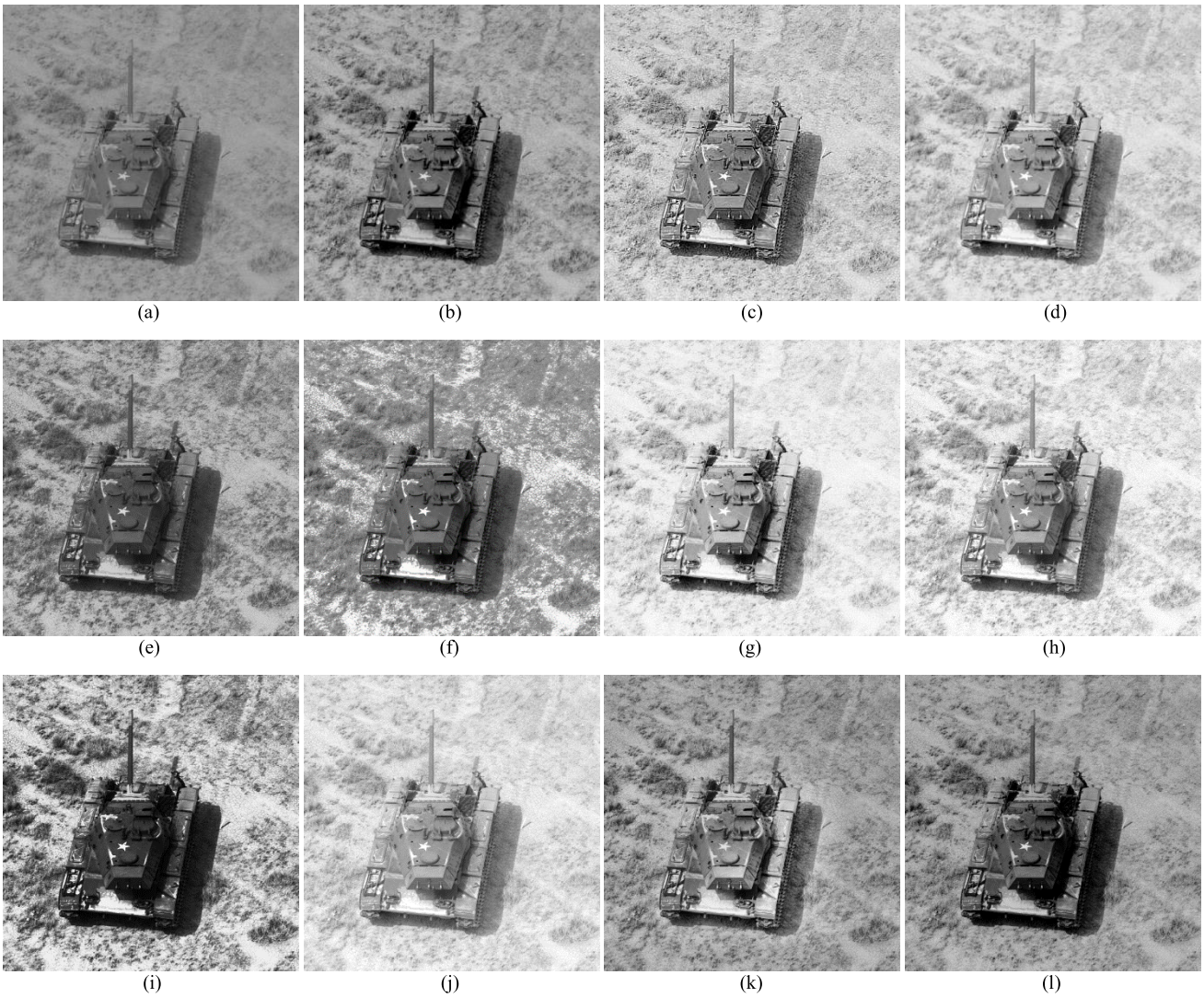

FIGURE 7. Enhanced images of the "Tank" image from the USC-SIPI database [42]: (a) input image, (b) NPEA [38], (c) LSCN [48], (d) RSIE [49], (e) WAHE [1], (f) CVC [20], (g) LDR [11], (h) AGC [23], (i) FCCE [45], (j) CESF [46], (k) EACE [47], and (l) proposed method.

mutual relationship between each pixel and its neighboring pixels.

B. SUBJECTIVE ASSESSMENT

Although an image has higher quantitative measures than other images, its subjective visual quality may not always superior accordingly [11], [45]. For this reason, this section presents examples of enhanced images for a subjective assessment of their visual qualities and conducts a comparative analysis of the properties of the proposed method and the conventional methods.

Fig. 5 demonstrates the enhanced images of the ''Giraffe'' image in Berkeley image dataset, which looks dull since pixel intensities are mainly distributed in the range of [90, 160]. In this figure, WAHE and EACE showed poor performance and NPEA, AGC, and CESF produced brightened images with low contrast. Whereas, CVC and FCCE caused visual artifacts due to over-enhancement in the background region. Although LSCN, RSIE, and LDR yielded good enhancement performance, the output images suffered from noise amplification in a sky region. On the other hand, the proposed method efficiently improved the image contrast while preventing considerable mean-brightness change or noise amplification.

Fig. 6 illustrates the enhanced images of the ''Eagles'' image in USC-SIPI database, which mainly consists of a sky region with similar pixel intensities in the range of [100, 140]. As shown in Fig. 6, RSIE, WAHE, CVC, LDR, FCCE, and EACE resulted in contouring artifacts in the sky region and NPEA produced the output image with poor contrast. In the cases of LSCN, AGC, and CESF, they gave excessively brightened images. On the other hand, the proposed method provided distinctive silhouettes of the eagles while preserving the mean-brightness of the input image.

In the case of the "Tank" image in Fig. 7, the input image suffers from low contrast since pixel intensities are mostly distributed in the range of [100, 160]. In LSCN, RSIE, LDR, AGC, and CESF, the mean-brightness values of the enhanced images were much higher than that of the input image. Even though CVC and FCCE achieved high enhancement performance, they produced visual artifacts caused by over-enhancement in the ground region. On the other hand, the proposed method improved image contrast without changing the mean-brightness and revealed hidden details of the tank.

V. CONCLUSION

We presented a novel contrast enhancement method using a sigmoid function based on the contrast sensitivity of the human retinal-photoreceptor. We modeled the contrast sensitivity as an exponential function of the log-intensity and derived a sigmoid function using the contrast sensitivity model. The optimal parameters for the proposed contrast enhancement method were estimated by employing a cost function that maximized the image contrast while preventing information loss. The proposed method not only had low computational complexity but also exhibited superior performance to state-of-the-art methods with regard to the contrast enhancement degree and mean-brightness/detail preservation. The proposed transformation function, which has the advantages of simplicity and effectiveness, may be applicable to other types of image processing such as tone mapping and low-light image enhancement. In future work, we will attempt to improve the detail-preservation performance of the proposed method by using local structural information such as a Retinex theory, 2-D histogram, or gradient distribution.

REFERENCES

[1] T. Arici, S. Dikbas, and Y. Altunbasak, "A histogram modification framework and its application for image contrast enhancement," *IEEE Trans. Image Process.*, vol. 18, no. 9, pp. 1921–1935, Sep. 2009.

[2] S. S. Agaian, K. Panetta, and A. M. Grigoryan, "Transform-based image enhancement algorithms with performance measure," *IEEE Trans. Image Process.*, vol. 10, no. 3, pp. 367–382, Mar. 2001.

[3] S. Agaian, B. Silver, and K. A. Panetta, "Transform coefficient histogram-based image enhancement algorithms using contrast entropy," *IEEE Trans. Image Process.*, vol. 16, no. 3, pp. 741–758, Mar. 2007.

[4] L. Dash and B. N. Chatterji, "Adaptive contrast enhancement and de-enhancement," *Pattern Recognit.*, vol. 24, no. 4, pp. 289–302, 1991.

[5] S. C. Nercessian, K. A. Panetta, and S. S. Agaian, "Non-linear direct multi-scale image enhancement based on the luminance and contrast masking characteristics of the human visual system," *IEEE Trans. Image Process.*, vol. 22, no. 9, pp. 3549–3561, Sep. 2013.

[6] S. Lee, "An efficient content-based image enhancement in the compressed domain using Retinex Theory," *IEEE Trans. Circuits Syst. Video Technol.*, vol. 17, no. 2, pp. 199–213, Feb. 2007.

[7] X. Fu, Y. Liao, D. Zeng, Y. Huang, X.-P. Zhang, and X. Ding, "A probabilistic method for image enhancement with simultaneous illumination and reflectance estimation," *IEEE Trans. Image Process.*, vol. 24, no. 12, pp. 4965–4977, Dec. 2015.

[8] H. Yue, J. Yang, X. Sun, F. Wu, and C. Hou, "Contrast enhancement based on intrinsic image decomposition," *IEEE Trans. Image Process.*, vol. 26, no. 8, pp. 3981–3994, Aug. 2017.

[9] E. H. Land and J. J. McCann, "Lightness and Retinex theory," *J. Opt. Soc. Amer.*, vol. 61, no. 1, pp. 1–11, 1971.

[10] T. Celik and T. Tjahjadi, "Automatic image equalization and contrast enhancement using Gaussian mixture modeling," *IEEE Trans. Image Process.*, vol. 21, no. 1, pp. 145–156, Jan. 2012.

[11] C. Lee, C. Lee, and C.-S. Kim, "Contrast enhancement based on layered difference representation of 2D histograms," *IEEE Trans. Image Process.*, vol. 22, no. 12, pp. 5372–5384, Dec. 2013.

[12] M. Kim and M. Chung, "Recursively separated and weighted histogram equalization for brightness preservation and contrast enhancement," *IEEE Trans. Consum. Electron.*, vol. 54, no. 3, pp. 1389–1397, Aug. 2008.

[13] Y.-T. Kim, "Contrast enhancement using brightness preserving bi-histogram equalization," *IEEE Trans. Consum. Electron.*, vol. 43, no. 1, pp. 1–8, Feb. 1997.

[14] Y. Wang, Q. Chen, and B. Zhang, "Image enhancement based on equal area dualistic sub-image histogram equalization method," *IEEE Trans. Consum. Electron.*, vol. 45, no. 1, pp. 68–75, Feb. 1999.

[15] S.-D. Chen and A. R. Ramli, "Contrast enhancement using recursive mean-separate histogram equalization for scalable brightness preservation," *IEEE Trans. Consum. Electron.*, vol. 49, no. 4, pp. 1301–1309, Nov. 2003.

[16] K. S. Sim, C. P. Tso, and Y. Y. Tan, "Recursive sub-image histogram equalization applied to gray scale images," *Pattern Recognit. Lett.*, vol. 28, no. 10, pp. 1209–1221, Jul. 2007.

[17] C. Wang and Z. Ye, "Brightness preserving histogram equalization with maximum entropy: A variational perspective," *IEEE Trans. Consum. Electron.*, vol. 51, no. 4, pp. 1326–1334, Nov. 2005.

[18] C. Wang, J. Peng, and Z. Ye, "Flattest histogram specification with accurate brightness preservation," *IET Image Process.*, vol. 2, no. 5, pp. 249–262, Oct. 2008.

[19] S.-W. Kim, B.-D. Choi, W.-J. Park, and S.-J. Ko, "2D histogram equalisation based on the human visual system," *Electron. Lett.*, vol. 52, no. 6, pp. 443–445, 2016.

[20] T. Celik and T. Tjahjadi, "Contextual and variational contrast enhancement," *IEEE Trans. Image Process.*, vol. 20, no. 12, pp. 3431–3441, Dec. 2011.

[21] T. Celik, "Two-dimensional histogram equalization and contrast enhancement," *Pattern Recognit.*, vol. 45, no. 10, pp. 3810–3824, Oct. 2012.

[22] T. Celik and L. Heng-Chao, "Residual spatial entropy-based image contrast enhancement and gradient-based relative contrast measurement," *J. Mod. Opt.*, vol. 63, no. 16, pp. 1600–1617, 2016.

[23] S.-C. Huang, F.-C. Cheng, and Y.-S. Chiu, "Efficient contrast enhancement using adaptive gamma correction with weighting distribution," *IEEE Trans. Image Process.*, vol. 22, no. 3, pp. 1032–1041, Mar. 2013.

[24] N. M. Kwok, Q. P. Ha, D. Liu, and G. Fang, "Contrast enhancement and intensity preservation for gray-level images using multiobjective particle swarm optimization," *IEEE Trans. Autom. Sci. Eng.*, vol. 6, no. 1, pp. 145–155, Jan. 2009.

[25] S. Rahman, M. M. Rahman, M. Abdullah-Al-Wadud, G. D. Al-Quaderi, and M. Shoyaib, "An adaptive gamma correction for image enhancement," *EURASIP J. Image Video Process.*, vol. 35, pp. 1–13, Dec. 2016.

[26] F. Kallel and A. B. Hamida, "A new adaptive gamma correction based algorithm using DWT-SVD for non-contrast CT image enhancement," *IEEE Trans. Nanobiosci.*, vol. 16, no. 8, pp. 666–675, Jan. 2017.

[27] S.-C. Huang and W.-C. Chen, "A new hardware-efficient algorithm and reconfigurable architecture for image contrast enhancement," *IEEE Trans. Image Process.*, vol. 23, no. 10, pp. 4426–4437, Oct. 2014.

[28] E. Reinhard, G. Ward, S. Pattanaik, and P. Debevec, *High Dynamic Range Imaging: Acquisition, Display, and Image-Based Lighting*. San Mateo, CA, USA: Morgan Kaufmann, 2005.

[29] Z. Chen, B. R. Abidi, D. L. Page, and M. A. Abidi, "Gray-level grouping (GLG): An automatic method for optimized image contrast Enhancement-part I: The basic method," *IEEE Trans. Image Process.*, vol. 15, no. 8, pp. 2290–2302, Aug. 2006.

[30] S.-D. Chen and A. R. Ramli, "Minimum mean brightness error bi-histogram equalization in contrast enhancement," *IEEE Trans. Consum. Electron.*, vol. 49, no. 4, pp. 1310–1319, Nov. 2003.

[31] G. Wyszecki and W. S. Stiles, *Color Science*. New York, NY, USA: Wiley, 1982.

[32] S. S. Stevens, "On the psychophysical law," *Psychol. Rev.*, vol. 64, no. 3, pp. 153–181, 1957.

[33] E. Reinhard, M. Stark, P. Shirley, and J. Ferwerda, "Photographic tone reproduction for digital images," *ACM Trans. Graph.*, vol. 21, no. 3, pp. 267–276, Jul. 2002.

[34] J. Tumblin, J. K. Hodgins, and B. K. Guenter, "Two methods for display of high contrast images," *ACM Trans. Graph.*, vol. 18, no. 1, pp. 56–94, 1999.

[35] S. Ferradans, M. Bertalmio, E. Provenzi, and V. Caselles, "An analysis of visual adaptation and contrast perception for tone mapping," *IEEE Trans. Pattern Anal. Mach. Intell.*, vol. 33, no. 10, pp. 2002–2012, Oct. 2011.

[36] E. Reinhard and K. Devlin, "Dynamic range reduction inspired by photoreceptor physiology," *IEEE Trans. Vis. Comput. Graphics*, vol. 11, no. 1, pp. 13–24, Jan. 2005.

[37] H. Su, C. Jung, S. Wang, and Y. Du, "Readability enhancement of displayed images under ambient light," *IEEE Trans. Circuits Syst. Video Technol.*, vol. 28, no. 7, pp. 1481–1496, Jul. 2018.

[38] S. Wang, J. Zheng, H.-M. Hu, and B. Li, "Naturalness preserved enhancement algorithm for non-uniform illumination images," *IEEE Trans. Image Process.*, vol. 22, no. 9, pp. 3538–3548, Sep. 2013.

[39] M. I. Sezan, K. L. Yip, and S. J. Daly, "Uniform perceptual quantization: Applications to digital radiography," *IEEE Trans. Syst., Man, Cybern. Syst.*, vol. SMC-17, no. 4, pp. 622–634, Jul. 1987.

[40] T. Cover and J. Thomas, *Elements of Information Theory*, 2nd ed. New York, NY, USA: Wiley, 2006.

[41] (2013). *Kodak Lossless True Color Image Suite*. [Online]. Available: http://r0k.us/graphics/kodak

[42] (2013). *USC-SIPI Database*. [Online]. Available: http://sipi.usc.edu/database

[43] P. Arbeláez, M. Maire, C. Fowlkes, and J. Malik, "Contour detection and hierarchical image segmentation," *IEEE Trans. Pattern Anal. Mach. Intell.*, vol. 33, no. 5, pp. 898–916, May 2011.

[44] W. Xue, L. Zhang, X. Mou, and A. C. Bovik, "Gradient magnitude similarity deviation: A highly efficient perceptual image quality index," *IEEE Trans. Image Process.*, vol. 23, no. 2, pp. 684–695, Feb. 2014.

[45] A. S. Parihar, O. P. Verma, and C. Khanna, "Fuzzy-contextual contrast enhancement," *IEEE Trans. Image Process.*, vol. 26, no. 4, pp. 1810–1819, Apr. 2017.

[46] N. Hassan and N. Akamatsu, "A new approach for contrast enhancement using sigmoid function," *Int. Arab. J. Inf. Technol.*, vol. 1, no. 2, pp. 221–226, 2004.

[47] S. Lal and M. Chandra, "Efficient algorithm for contrast enhancement of natural images," *Int. Arab J. Inf. Technol.*, vol. 11, no. 1, pp. 95–102, 2014.

[48] K. Zhan, J. Shi, J. Teng, Q. Li, M. Wang, and F. Lu, "Linking synaptic computation for image enhancement," *Neurocomputing*, vol. 238, pp. 1–12, May 2017.

[49] X. Fu, J. Wang, D. Zeng, Y. Huang, and X. Ding, "Remote sensing image enhancement using regularized-histogram equalization and DCT," *IEEE Geosci. Remote Sens. Lett.*, vol. 12, no. 11, pp. 2301–2305, Nov. 2015.

[50] W. H. Press, B. P. Flannery, S. A. Teukolsky, and W. T. Vetterling, *Numerical Recipes*. Cambridge, U.K.: Cambridge Univ. Press, 1988.

[51] C. Liu, X. Sui, X. Kuang, Y. Liu, G. Gu, and Q. Chen, "Optimized contrast enhancement for infrared images based on global and local histogram specification," *Remote Sens.*, vol. 11, no. 7, p. 849, 2019.

[52] H.-T. Wu, W. Mai, S. Meng, Y.-M. Cheung, and S. Tang, "Reversible data hiding with image contrast enhancement based on two-dimensional histogram modification," *IEEE Access*, vol. 7, pp. 83332–83342, 2019.

[53] B. Subramani and M. Veluchamy, "Fuzzy contextual inference system for medical image enhancement," *Measurement*, vol. 148, Dec. 2019, Art. no. 106967.

[54] T. Qiu, C. Wen, K. Xie, F.-Q. Wen, G.-Q. Sheng, and X.-G. Tang, "Efficient medical image enhancement based on CNN-FBB model," *IET Image Process.*, vol. 13, no. 10, pp. 1736–1744, 2019.

[55] M. Li, S. Shen, W. Gao, W. Hsu, and J. Cong, "Computed tomography image enhancement using 3D convolutional neural network," in *Deep Learning in Medical Image Analysis and Multimodal Learning for Clinical Decision Support*. Cham, Switzerland: Springer, 2018, pp. 291–299.

[56] K. G. Lore, A. Akintayo, and S. Sarkar, "LLNet: A deep autoencoder approach to natural low-light image enhancement," *Pattern Recognit.*, vol. 61, pp. 650–662, Jan. 2017.

[57] W. Ren, S. Liu, L. Ma, Q. Xu, X. Xu, X. Cao, J. Du, and M.-H. Yang, "Low-light image enhancement via a deep hybrid network," *IEEE Trans. Image Process.*, vol. 28, no. 9, pp. 4364–4375, Sep. 2019.

[58] J. Li, G. Li, and H. Fan, "Image dehazing using residual-based deep CNN," *IEEE Access*, vol. 6, pp. 26831–26842, 2018.

[59] C. Hodges, M. Bennamoun, and H. Rahmani, "Single image dehazing using deep neural networks," *Pattern Recognit. Lett.*, vol. 128, pp. 70–77, Dec. 2019.

[60] Z. Huang, Y. Zhang, Q. Li, T. Zhang, N. Sang, and H. Hong, "Progressive dual-domain filter for enhancing and denoising optical remote-sensing images," *IEEE Geosci. Remote Sens. Lett.*, vol. 15, no. 5, pp. 759–763, May 2018.

[61] Y. Wang, H. Wang, C. Yin, and M. Dai, "Biologically inspired image enhancement based on Retinex," *Neurocomputing*, vol. 177, no. 177, pp. 373–384, Feb. 2016.

[62] Z. Huang, L. Huang, Q. Li, T. Zhang, and N. Sang, "Framelet regularization for uneven intensity correction of color images with illumination and reflectance estimation," *Neurocomputing*, vol. 314, pp. 154–168, Nov. 2018.

[63] Z. Huang, H. Fang, Q. Li, Z. Li, T. Zhang, N. Sang, and Y. Li, "Optical remote sensing image enhancement with weak structure preservation via spatially adaptive gamma correction," *Infr. Phys. Technol.*, vol. 94, pp. 38–47, Nov. 2018.

SEUNG PARK received the B.S. degree in electrical engineering from Korea University, Seoul, South Korea, in 2013, where he is currently pursuing the Ph.D. degree. He joined the Computer Vision and Image Processing Laboratory, Department of Electrical Engineering, Korea University, in March 2013. His current research interests include image processing, contrast enhancement, visual tracking, and visual odometry.

YONG-GOO SHIN received the B.S. degree in electrical engineering from Korea University, in 2014, where he is currently pursuing the Ph.D. degree in electrical engineering. His current research interests include human–computer interfaces, digital signal processing, computer vision, and artificial intelligence.

SUNG-JEA KO (M'88–SM'97–F'12) received the B.S. degree in electronic engineering from Korea University, in 1980, and the M.S. and Ph.D. degrees in electrical and computer engineering from The State University of New York at Buffalo, Buffalo, in 1986 and 1988, respectively.

From 1988 to 1992, he was an Assistant Professor with the Department of Electrical and Computer Engineering, University of Michigan–Dearborn. In 1992, he joined the Department of Electronic Engineering, Korea University, where he is currently a Professor. He has published more than 200 international journal articles. He also holds more than 60 registered patents in fields, such as video signal processing and computer vision.

Prof. Ko was a recipient of the Best Paper Award from the IEEE Asia Pacific Conference on Circuits and Systems, in 1996, the Hae-Dong Best Paper Award from the Institute of Electronics and Information Engineers (IEIE), in 1997, the LG Research Award, in 1999, the Research Excellence Award from Korea University, in 2004, and the Technical Achievement Award from the IEEE Consumer Electronics (CE) Society, in 2012. He was also a recipient of the 15-year Service Award from the TPC of ICCE, in 2014, and the Chester Sall Award from the IEEE CE Society, in 2017. He has served as the General Chairman of the ITC-CSCC 2012 and the IEICE 2013. He is a member of the Editorial Board of the IEEE TRANSACTIONS ON CONSUMER ELECTRONICS. He was the President of the IEIE, in 2013, and the Vice-President of the IEEE CE Society, from 2013 to 2016. He is currently a Distinguished Lecturer of the IEEE.